

Temperature Fluctuation Profiles in Turbulent Thermal Convection: A Logarithmic Dependence versus a Power-Law Dependence

Yu-Hao He (何宇昊)¹ and Ke-Qing Xia (夏克青)^{1,2,*}

¹*Department of Physics, The Chinese University of Hong Kong, Shatin, Hong Kong, China*

²*Center for Complex Flows and Soft Matter Research and Department of Mechanics and Aerospace Engineering, Southern University of Science and Technology, Shenzhen, Guangdong 518055, China*



(Received 21 April 2018; published 10 January 2019)

We report an experimental measurement of the rms temperature (σ_T) profiles in two regions inside a large aspect ratio ($\Gamma = 4.2$) rectangular convection cell. It is found that, in the region where the boundary layer is sheared by a large-scale wind, σ_T has a power-law dependence on the vertical distance (z) from the plate, whereas in the region where plumes are abundant, σ_T has a logarithmic dependence on z . The power-law profile may be understood by balancing the inertia force and the viscous force in the equations of motion, and the logarithmic profile may be understood in terms of the balance between the buoyancy and the inertia forces. When normalized by a convective temperature scale, θ_c , the profiles of σ_T collapse onto a single curve for different values of the Rayleigh number. This shows that the convective temperature first proposed by Deardorff is the suitable temperature scale outside the thermal boundary layer for both logarithmic and power-law profiles. Our finding suggests a strong connection between plumes and the logarithmic rms temperature profile. The present Letter reveals that multiple force balance mechanisms can coexist in the bulk of highly turbulent flows.

DOI: [10.1103/PhysRevLett.122.014503](https://doi.org/10.1103/PhysRevLett.122.014503)

The shape of velocity and temperature profiles in turbulent flows above a surface determines the momentum and heat transport in the region concerned, and they in turn are determined by the balance of the various force terms in the related equations of motion. An example is the classical work of Priestley on natural convection over a flat surface that models the atmospheric boundary layer (ABL); using a similarity argument, he suggested that the root-mean-square (rms) temperature profile has a power-law dependence on the distance from the surface, i.e., $\sigma_T \sim z^{-1/3}$ [1]. In the late 1980s, and in connection to turbulent thermal convection, a scaling theory was proposed by Castaing *et al.* to explain the observed heat transport property from convection experiments [2]. Based on the scaling model of Castaing *et al.*, Adrian obtained different types of the rms temperature profiles [3]. Depending on which of the two scenarios proposed in the Castaing *et al.* model, the profile can take either logarithmic or power-law form. Assuming their velocity matches the fluctuating velocity of the core as the plumes enter the bulk from the so-called convective layer (or mixing zone), Adrian derived a power-law profile for the rms temperature, i.e., $\sigma_T \sim z^{-1/2}$, and termed this the λ -I model. If, on the other hand, it is the temperature scale of the mixing zone that matches the fluctuating temperature of the bulk, then one obtains a logarithmic profile, i.e., $\sigma_T \sim \ln(z)$, which Adrian called λ -II model. Although based on different assumptions and physical pictures, both models produce a logarithmic profile for the rms velocity and the same scaling for the global heat transport,

i.e., $\text{Nu} \sim \text{Ra}^{2/7}$, where the Nusselt number Nu is the nondimensional heat flux and Ra the Rayleigh. As shown by Adrian, these two models imply different local force balances; the λ -I model implies a balance between the inertia and viscous forces and the λ -II model implies a balance between buoyancy and inertia forces. The predictions, either the one by Priestley or the ones by Adrian, however, have not been unambiguously verified by experiments. Limited by either measurement precision or the range of distance, some of the earlier experiments were not able to convincingly distinguish between power law and logarithmic profiles [4–7]. In some of the more recent studies, power-law scaling was observed [8–11], but the reported scaling exponent from different studies was quite different from one another and for the same study the exponent was found to depend on both Ra and the aspect ratio of the apparatus.

In this Letter we report experimental measurements of the rms temperature profile in turbulent Rayleigh-Bénard convection (RBC), a paradigmatic system widely used in studying thermally driven turbulent flows in nature [12–15]. Three control parameters are used to characterize this system: the Rayleigh number $\text{Ra} = \beta g \Delta T H^3 / \nu \kappa$, the Prandtl number $\text{Pr} = \nu / \kappa$, and the aspect ratio $\Gamma = L / H$, where g is the gravitational acceleration, H and L correspond to the height and lateral length of the system, ΔT is the temperature difference across the fluid layer, and β , ν , κ are the volume expansion coefficient, kinematic viscosity, and thermal diffusivity of the working fluid, respectively.

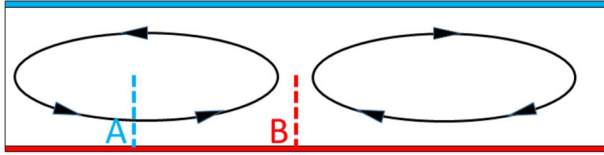


FIG. 1. Schematic drawing of experimental apparatus. A: shear-dominated region; B: plume-abundant region.

In the experiment Ra varied from 3.2×10^7 to 2×10^8 . The lower and upper limits of the Rayleigh number were chosen such that a well-organized large-scale circulation would be present in the convective flow while the non-Oberbeck-Boussinesq effect remains negligible. Degassed and deionized water was used as the working fluid and maintained at a mean temperature of 40°C ($Pr = 4.34$). The cell was placed in a thermostat maintained at $T = 40^\circ\text{C}$.

The convection cell is of a rectangular shape with its length L , width W , and height H equal to $249 \times 75 \times 59$ (mm), respectively, so the aspect ratios in the length direction is $\Gamma = L/H = 4.2$, and that in the width direction is 1.3. The top and bottom plates of the cell are made of copper and the sidewall Plexiglas. For other details of the cell, we refer to Ref. [16]. A schematic sketch of the convection cell is shown in Fig. 1. The geometry of the convection cell offers two major advantages. The first one is that, with the quasi-2D geometry, the large-scale circulation (LSC) would be largely confined in a vertical plane [16]. This would eliminate the azimuthal motion of the LSC and reduce the associated temperature fluctuations arising from the stochastic dynamics of LSC such as its azimuthal meandering, sloshing, and torsional motions [17–21]. The second one is, as the measurement regions are far from sidewall, the impact from sidewall on the rms temperature profile can be eliminated. It is known that with this Γ the LSC would be a two-roll structure [22]. We can then identify two regions with different flow dynamics. In the first region, the thermal boundary layer is sheared by a large-scale wind, which can be regarded as a shear-dominated region (marked by “A” in Fig. 1, midway between the left sidewall and cell center), while in another region, the plumes concentrate and move upwards, which is called plume-abundant region (marked by “B” in Fig. 1, at cell center). rms temperature profiles were measured in these two regions (see red and blue dashed lines in Fig. 1), using a thermistor (~ 0.3 mm in size) attached to a movable thin stainless steel tube. The vertical measuring positions were from 0.7 mm to 29.4 mm and the measurement time at each vertical position varied from 1 to 2 hours, which corresponds to 14 244 to 18 711 free-fall time unit for the lowest and highest Rayleigh number, respectively.

Plotted in Fig. 2 are temperature time series taken at the shear-dominant and plume-dominant regions and at two heights from the bottom plate, $z/\lambda_{th} \approx 2$ (left panel) and $z/\lambda_{th} \approx 20$ (right panel), respectively. The thermal boundary layer thickness, λ_{th} , estimated using the

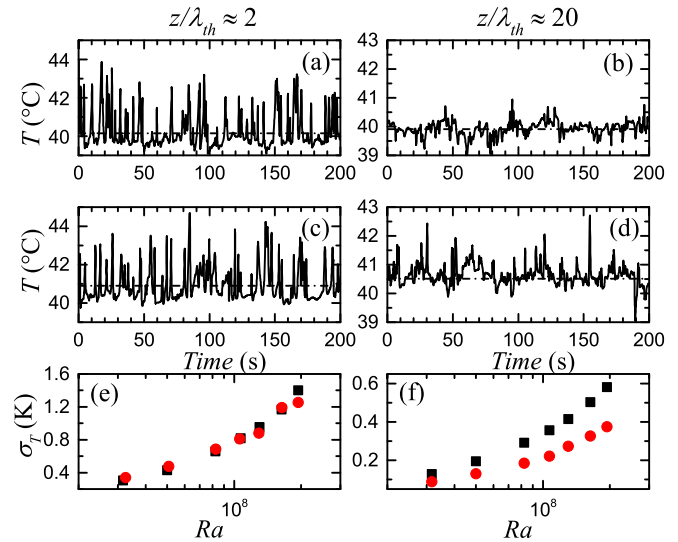


FIG. 2. (a)–(d) Temperature time series measured at $Ra \approx 1.1 \times 10^8$. Top panel: in the wind-shearing region A. Middle panel: in the plume-abundant region B. (e) and (f) rms temperature versus Ra ; circles: data taken in region A; squares: data taken in region B.

equation $\lambda_{th} = H/2Nu$, equals 1.0 mm for the present Ra ($\approx 1.1 \times 10^8$). Figures 2(a) and 2(c) show that, very close to the bottom plate, the temperature signal is characterized by intense upward peaks, which are signatures of hot plumes detaching from thermal BL. Figures 2(b) and 2(d), on the other hand, show that, away from the BL, the fluctuations in the plume-abundant region B is much stronger than in the shear-dominated region A. This is quantified by the rms temperature measured at the near-center height $z/\lambda_{th} \approx 20$ in the two respective regions for different values of Ra , as shown in Fig. 2(f). In the figure, circles were measured from region A and squares from region B. The figure also shows that fluctuation intensity in the plume-dominant region increases faster with Ra than that in the shear-dominant region. In contrast, as shown in Fig. 2(e), near the BL, the rms value measured in the two regions are comparable in magnitude for all Ra values. Figure 3 shows the probability density function of the normalized temperature fluctuations for seven Rayleigh numbers corresponding to the same positions as in Fig. 2. We see that, near the BL, the PDFs from the regions A and B are very similar, both are positively skewed owing to the emission of hot plumes. Whereas, near the center PDFs from the plume-abundant region B are much more skewed toward the positive. These results are consistent with those from Fig. 2. It is also seen that the PDFs for different Ra collapse on top of each other, this is an indication that the flow pattern remains the same for all values of Ra . Figures 2 and 3 show that very close to the boundary layer the measured temperature signals from the shear-dominated and plume-abundant regions are rather similar, whereas away from the BL they are very different for the two

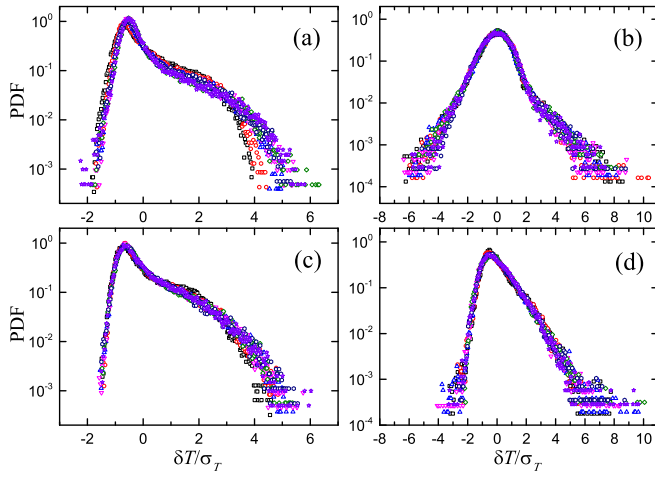


FIG. 3. Probability density function of the normalized temperature fluctuations for all Ra values. Upper panel: in the shear-dominated region A. Lower panel: in the plume-abundant region B. Left panel: data taken at $z/\lambda_{th} \approx 2$. Right panel: at $z/\lambda_{th} \approx 20$.

regions. This reflects the different flow dynamics in the two regions above the BL.

We now examine the rms temperature profiles. Figure 4(a) plots σ_T versus z measured in the wind-shearing region A for different Ra in a log-log scale. It is well-known that the rms temperature profile in turbulent convection first increases and then decreases when moving away from the plate, with its peak position roughly coinciding with the edge of the thermal BL, so that this peak position can also be used as an alternative measure of the BL [5,23]. As the related theoretical models all concern profiles in the convective layer or mixing zone, we shall focus on data points outside the thermal BL, i.e., those points beyond the peak position (shown as solid symbols in the figure). The solid lines in Fig. 4(a) represent power-law fits to the respective data set. The fitting for most cases cover a vertical range of over one decade (from $z = 1.4$ mm to $z = 20.7$ mm), with the obtained scaling exponent α ($\sigma_T \approx z^\alpha$), varies from 0.55 to 0.62. Note that the data points at $z = 30$ mm (corresponding to cell center position) do not follow the power law. It is known that turbulent temperature and velocity fluctuations are nearly homogeneous and isotropic in the central region of the cell [6,24,25], so temperature fluctuations close to the cell center show no positional dependence.

Since most of the data used in the fitting are far away from the BL, molecular conductivity would be less important. We use the so-called Deardorff convective temperature scale [26], defined as $\theta_* = Q_0 / (Q_0 g \beta H)^{1/3}$, and the height of the fluid layer, H , as characteristic temperature and length scales for normalization. Here, Q_0 is the total heat flux transported in the system. In Fig. 4(b), we plot the normalized temperature fluctuation σ_T/θ_* versus the normalized vertical distance z/H . We see that outside the BL the profiles collapse nicely onto a single curve after

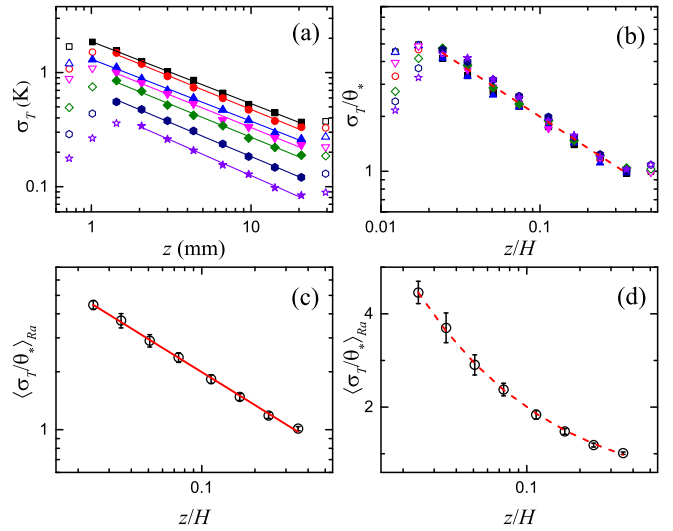


FIG. 4. Measured rms temperature profiles in the shear-dominated region A: (a) Log-log plot of rms temperature σ_T versus vertical position, z . The solid symbols are data points used in the fitting. From top to bottom, the corresponding Ra are as follows: 1.94×10^8 , 1.64×10^8 , 1.29×10^8 , 1.06×10^8 , 8.25×10^7 , 5.08×10^7 , and 3.25×10^7 . (b) Log-log plot of normalized rms temperature σ_T/θ_* versus normalized vertical position, z/H . (c) Log-log plot of the normalized rms temperature averaged over Ra, $\langle \sigma_T/\theta_* \rangle_{Ra}$, versus z/H . (d) The same data as in (c) but in a semilog scale.

normalization, indicating universality for normalized σ_T profiles with respect to Ra. As σ_T/θ_* shows no dependence on Ra, we average the solid data points in Fig. 4(b) for the respective vertical positions, and denote them as $\langle \sigma_T/\theta_* \rangle_{Ra}$. Figure 4(c) shows a log-log plot of the resultant $\langle \sigma_T/\theta_* \rangle_{Ra}$ versus z/H . The solid line represents a power-law fit to the data, $\langle \sigma_T/\theta_* \rangle_{Ra} = 0.54(z/H)^{-0.57 \pm 0.01}$ [for reference, the same line is also shown in Figs. 4(b) and 4(d)]. The error bars in the figure are the standard deviations of σ_T/θ_* for different Ra and the maximum fitting error is less than 4%. For comparison, we plot the same data in semilog scale in Fig. 4(d), which clearly shows that the rms temperature profile in the wind-shearing region does not have a logarithmic dependence on distance. The absolute value of the power-law exponent obtained here is larger than either the $-1/3$ predicted by Priestley's self-similarity theory [27] or the $-1/2$ predicted by Adrian's λ -I model [3], but is closer to the latter.

Figure 5(a) plots the temperature rms profiles measured in the plume-abundant region B in semilog scale. Again, we focus on regions outside the BL. The lines in the figure represent the logarithmic fits to the individual data sets, with the distance varying over one decade. Applying the same normalization as before, we plot σ_T/θ_* versus z/H in Fig. 5(b). The nice collapse of data points shows that there is universality for the normalized rms temperature profiles with respect to Ra in the plume-abundant region as well. Again, we average the solid symbols in Fig. 5(b) for the

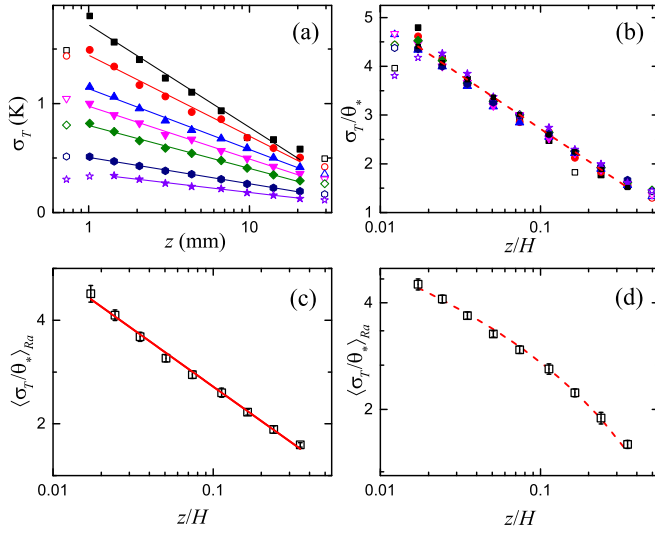


FIG. 5. Measured rms temperature profiles in plume-dominated region: (a) Semilog plot of rms temperature σ_T , versus vertical position, z . The solid symbols are data points used in the fitting. The legends for different Ra are the same as in Fig. 4. (b) Semilog plot of normalized rms temperature σ_T/θ_* versus normalized vertical position, z/H . (c) Semilog plot of the normalized rms temperature averaged over Ra, $\langle \sigma_T/\theta_* \rangle_{Ra}$, versus z/H . (d) The same data as in (c) but in log-log plot.

respective vertical positions and plot the resultant $\langle \sigma_T/\theta_* \rangle_{Ra}$ versus z/H in Fig. 5(c) in a semilog scale, with the error bars obtained in the same way as before. The solid line in the figure represents $\langle \sigma_T/\theta_* \rangle_{Ra} = -0.92 \ln(z/H) + 0.59$ [for reference the same fitting is shown in Figs. 5(b) and 5(d) as the dashed line]. The maximum fitting error is less than 3%. For comparison, we plot the same data in the log-log scale in Fig. 5(d), which shows unambiguously that the rms temperature profile in the plume-abundant region cannot be described by a power law relationship. Also note that, for both the plume- and shear-dominated regions, the Deardorff convective temperature scale, while nicely collapsing data in the mixing zone and the bulk, cannot collapse data inside the thermal BL [see Figs. 4(b) and 5(b)], as expected.

As the power-law and log profiles are derived with different assumptions and imply different force balances, we evaluate the related quantities. The basic assumption made for the λ -I model is that the typical velocity scale in the BL ($V_b = \beta g \Delta T \lambda_{th}^2 / \nu$) matches that in the convective core [$V_* = (Q_0 \beta g H)^{1/3}$]. Substituting the respective quantities and using our measured Nu-Ra relation [$Nu = Q_0 H / (\kappa \Delta T) = 0.16 Ra^{0.28}$], we obtain $V_b = 2.51 \times 10^{-5} Ra^{0.44}$ (m/s) and $V_* = 2.28 \times 10^{-6} Ra^{0.43}$ (m/s), with V_b being roughly ten times larger than V_* . For the λ -II model, the key assumption is that the temperature scale in the BL ($\theta_b = \kappa \nu / \beta g \lambda_{th}^3$) is the same as that in the core region (θ_*). Evaluating these quantities using our measured data, we find $\theta_b = 4.21 \times 10^{-9} Ra^{0.84}$ (K) and $\theta_* = 2.32 \times 10^{-8} Ra^{0.85}$ (K), with the magnitude of θ_*

about 5 times larger than θ_b . Given that these are order-of-magnitude scaling arguments, we see that the key assumptions for both the λ -I and λ -II models hold approximately, at least scaling wise.

The above results show very convincingly that both logarithmic and power-law rms temperature profiles can be present in turbulent convection at the same time but in different regions of the bulk, depending on the local flow conditions. This shows that there is no single force balance mechanism at work in this complicated system, rather, the balance is local. Thus, assuming either a log or a power-law profile existing in the system is a too simplistic approach. We note that the design of our apparatus greatly reduces the influences from the sidewall and the stochastic motions of the LSC. This specific apparatus coupled with the high measurement precision enabled us to unambiguously distinguish and disentangle the logarithmic and power-law profiles, which has remained an unsettled issue until now. It should be noted that logarithmic profile for the mean temperature has been observed in regions where plumes are emitted [28]. As the mean temperature log profile has been associated with the boundary layer being turbulent [29–31], the authors of the above work have argued that the plume-emitting region of the BL may be turbulent. In our case, the Ra values are too low for the BL to be turbulent. So the logarithm observed in the two cases may be for different reasons. But it is clear that they are all related to the local plume dynamics.

In summary, our experiment has convincingly show that two distinct rms temperature profiles can coexist in a Rayleigh-Bénard convection cell. In the shear-dominated region, the profile is well-fitted by a power law, while a clearly logarithmic profile is found in the plume-dominated region. In both cases, we find the profiles to be invariant with respect to Ra once they are scaled by the Deardorff convective temperature scale and the distance by the depth of the convecting fluid. This is the first time that both logarithmic and the power-law rms temperature profiles have been unambiguously measured in different regions inside a single turbulent thermal convection cell. Our results also show that the convective temperature first proposed by Deardorff almost 50 years ago for the ABL is the characteristic temperature scale in the mixing zone and the bulk for both plume- and shear-dominated regions, but not inside the thermal BL. As regions of shearing-wind and rising-thermals both exist in an ABL [32], the present results may have potential implications for atmospheric research. The fact that different types of force balance can coexist in the same system shows that assuming a single physical mechanism applicable to the whole cell in a complex system such as the Rayleigh-Bénard convection may be an over-simplified approach. Rather, different regions can have their own dynamics, even if the locations are all in the convective layer (or bulk), the local dynamics can be very different.

We gratefully acknowledge support of this work by the Hong Kong Research Grants Council under Projects No. CUHK14301115 and No. CUHK14302317.

*Corresponding author.
xiakq@sustc.edu.cn

- [1] H.-B. Priestley, Free and forced convection in the atmosphere near the ground, *Q. J. R. Meteorol. Soc.* **81**, 139 (1955).
- [2] B. Castaing, G. Gunaratne, F. Heslot, L. Kadanoff, A. Libchaber, S. Thomae, X.-Z. Wu, S. Zaleski, and G. Zanetti, Scaling of hard thermal turbulence in Rayleigh-Bénard convection, *J. Fluid Mech.* **204**, 1 (1989).
- [3] R. Adrian, Variation of temperature and velocity fluctuations in turbulent thermal convection over horizontal surfaces, *Int. J. Heat Mass Transfer* **39**, 2303 (1996).
- [4] A. A. Townsend, Temperature fluctuations over a heated horizontal surface, *J. Fluid Mech.* **5**, 209 (1959).
- [5] A. Tilgner, A. Belmonte, and A. Libchaber, Temperature and velocity profiles of turbulent convection in water, *Phys. Rev. E* **47**, R2253 (1993).
- [6] A. Belmonte, A. Tilgner, and A. Libchaber, Temperature and velocity boundary layers in turbulent convection, *Phys. Rev. E* **50**, 269 (1994).
- [7] R. L. J. Fernandes and R. J. Adrian, Scaling of velocity and temperature fluctuations in turbulent thermal convection, *Exp. Therm. Fluid. Sci.* **26**, 355 (2002).
- [8] A. Maystrenko, C. Resagk, and A. Thess, Structure of the thermal boundary layer for turbulent Rayleigh-Bénard convection of air in a long rectangular enclosure, *Phys. Rev. E* **75**, 066303 (2007).
- [9] R. du Puits, C. Resagk, A. Tilgner, F. H. Busse, and A. Thess, Structure of thermal boundary layers in turbulent Rayleigh-Bénard convection, *J. Fluid Mech.* **572**, 231 (2007).
- [10] C. Sun, Y.-H. Cheung, and K.-Q. Xia, Experimental studies of the viscous boundary layer properties in turbulent Rayleigh-Bénard convection, *J. Fluid Mech.* **605**, 79 (2008).
- [11] P. Wei and G. Ahlers, On the nature of fluctuations in turbulent Rayleigh-Bénard convection at large Prandtl numbers, *J. Fluid Mech.* **802**, 203 (2016).
- [12] G. Ahlers, S. Grossmann, and D. Lohse, Heat transfer and large scale dynamics in turbulent Rayleigh-Bénard convection, *Rev. Mod. Phys.* **81**, 503 (2009).
- [13] D. Lohse and K.-Q. Xia, Small-scale properties of turbulent Rayleigh-Bénard convection, *Annu. Rev. Fluid Mech.* **42**, 335 (2010).
- [14] F. Chillà and J. Schumacher, New perspectives in turbulent Rayleigh-Bénard convection, *Eur. Phys. J. E.* **35**, 58 (2012).
- [15] K.-Q. Xia, Current trends and future directions in turbulent thermal convection, *Theor. Appl. Mech. Lett.* **3**, 052001 (2013).
- [16] K.-Q. Xia, C. Sun, and S.-Q. Zhou, Particle image velocimetry measurement of the velocity field in turbulent thermal convection, *Phys. Rev. E* **68**, 066303 (2003).
- [17] H.-D. Xi, Q. Zhou, and K.-Q. Xia, Azimuthal motion of the mean wind in turbulent thermal convection, *Phys. Rev. E* **73**, 056312 (2006).
- [18] H.-D. Xi, S.-Q. Zhou, Q. Zhou, T.-S. Chan, and K.-Q. Xia, Origin of the Temperature Oscillation in Turbulent Thermal Convection, *Phys. Rev. Lett.* **102**, 044503 (2009).
- [19] Q. Zhou, H.-D. Xi, S.-Q. Zhou, C. Sun, and K.-Q. Xia, Oscillations of the large-scale circulation in turbulent Rayleigh-Bénard convection: The sloshing mode and its relationship with the torsional mode, *J. Fluid Mech.* **630**, 367 (2009).
- [20] C. Sun, H.-D. Xi, and K.-Q. Xia, Azimuthal Symmetry, Flow Dynamics, and Heat Transport in Turbulent Thermal Convection in a Cylinder with an Aspect Ratio of 0.5, *Phys. Rev. Lett.* **95**, 074502 (2005).
- [21] D. Funfschilling and G. Ahlers, Plume Motion and Large-Scale Circulation in a Cylindrical Rayleigh-Bénard Cell, *Phys. Rev. Lett.* **92**, 194502 (2004).
- [22] K.-Q. Xia, C. Sun, and Y.-H. Cheung, Large Scale Velocity Structures in Turbulent Thermal Convection with Widely Varying Aspect Ratio, *14th International Symposium on Applications of Laser Techniques to Fluid Mechanics* (2008).
- [23] S.-L. Lui and K.-Q. Xia, Spatial structure of the thermal boundary layer in turbulent convection, *Phys. Rev. E* **57**, 5494 (1998).
- [24] C. Sun, Q. Zhou, and K.-Q. Xia, Cascades of Velocity and Temperature Fluctuations in Buoyancy-Driven Thermal Turbulence, *Phys. Rev. Lett.* **97**, 144504 (2006).
- [25] Q. Zhou, C. Sun, and K.-Q. Xia, Experimental investigation of homogeneity, isotropy, and circulation of the velocity field in buoyancy-driven turbulence, *J. Fluid Mech.* **598**, 361 (2008).
- [26] J. W. Deardorff, Convective velocity and temperature scales for the unstable planetary boundary layer and for Rayleigh convection, *J. Atmos. Sci.* **27**, 1211 (1970).
- [27] C. H. B. Priestley, *Turbulent Transport in the Lower Atmosphere* (University of Chicago Press, Chicago, 1959).
- [28] E. P. van der Poel, R. Ostilla-Mónico, R. Verzicco, S. Grossmann, and D. Lohse, Logarithmic Mean Temperature Profiles and Their Connection to Plume Emissions in Turbulent Rayleigh-Bénard Convection, *Phys. Rev. Lett.* **115**, 154501 (2015).
- [29] G. Ahlers, E. Bodenschatz, D. Funfschilling, S. Grossmann, X. He, D. Lohse, R. Stevens, and R. Verzicco, Transition to the Ultimate State of Turbulent Rayleigh-Bénard Convection, *Phys. Rev. Lett.* **109**, 114501 (2012).
- [30] P. Wei and G. Ahlers, Logarithmic temperature profiles in the bulk of turbulent Rayleigh-Bénard convection for a Prandtl number of 12.3, *J. Fluid Mech.* **758**, 809 (2014).
- [31] G. Ahlers, E. Bodenschatz, and X. Z. He, Logarithmic temperature profiles of turbulent Rayleigh-Bénard convection in the classical and ultimate state for a Prandtl number of 0.8, *J. Fluid Mech.* **758**, 436 (2014).
- [32] R. B. Stull, *An Introduction to Boundary Layer Meteorology* (Kluwer Academic Publishers, Dordrecht, 2012).